Electronic Supplementary Material (ESI) for Journal of Materials Chemistry A.
This journal is © The Royal Society of Chemistry 2019

Supporting Information for

A two-dimensional semiconducting covalent organic framework with nickel(II) coordination for high capacitive performance

Tao Li,[a] Wen-Da Zhang,[a] Yong Liu,[a] Yunxing Li,[a] Caikun Cheng,[a] Haiyan Zhu,[a] Xiaodong Yan,[a] Zaijun Li,*[a] and Zhi-Guo Gu*[ab]*

[a] Key Laboratory of Synthetic and Biological Colloids, Ministry of Education, School of Chemical and Material Engineering, Jiangnan University, Wuxi 214122, China

[b] International Joint Research Center for Photoresponsive Molecules and Materials, School of Chemical and Material Engineering, Jiangnan University, Wuxi 214122, China

E-mail: zhiguogu@jiangnan.edu.cn

1. General Information

All reagents and solvents were reagent grade, purchased from commercial sources and used without further purification. Fourier transform infrared (FT-IR) spectra were performed on a Thermo Nicolet iS10 spectrometer in the spectral range of 500-4000 cm^{-1}. ^{13}C cross-polarization with magic angle-spinning (CP-MAS) solid-state nuclear magnetic resonance (NMR) spectra were recorded on a Bruker ARX 300 MHz spectrometer. Mass spectra (MS) were taken on a Waters MALDI SYNAPT G2 Series spectrometer. X-ray photoelectron spectroscopy (XPS) analysis was measured by a Kratos Axis Supra instrument (Kratos Analytical, Manchester, UK) using a monochromatized Al Ka radiation as X-ray source. Thermogravimetric analyses (TGA) were obtained using a Mettler Toledo TGA/DSC1/1100SF analyser in the temperature range of 30 to 800 °C under flowing N_2. The Brunauer-Emmett-Teller (BET) surface areas were observed on N_2 sorption isotherms at 77 K using a Micromeritics ASAP2020 surface area and pore size analyser. Pore size distribution was determined by nonlocal density functional theory mode in the instrument software package. Scanning electron microscopy (SEM) images were obtained on a Hitachi S-4800. Transmission electron microscopy (TEM) images were observed on a JEOL JEM-2100. Scanning transmission electron microscopy (STEM) images, HRTEM images and EDS mapping were carried out on a Tecnai G2 F30 transmission electron microscopy at an acceleration voltage of 300 kV. Powder electrical conductivity was recorded on a Suzhou Jingge ST2253 by four-probe method. Thin film electrical conductivity was measured by the van der Pauw method under temperature control, the date was collected using a Keithley 4200-SCS parameter analyzer.

2. Electrochemical performance experiments

The electrochemical performances of the samples were carried out on an electrochemical station (CHI660E). Cyclic voltammetry (CV), galvanostatic charge-discharge (GCD) and Electrochemical impedance spectroscopy (EIS) measurement were conducted on in a three-electrode setup, including a Pt plate (1 cm^2) as the counter electrode and Hg/HgO electrode as the reference electrode. The working electrode was prepared by mixing active material, acetylene black and poly(tetrafluoethylene) in a mass ratio of 8:1:1, and then dispersed in ethanol by ultrasonication to obtain homogeneous slurry. The slurry was coated on a Ni foam substrate (1 cm^2). The mass loading of active materials on Ni foam was 5.0 mg cm^{-2}. Moreover, the asymmetric supercapacitor devices were assembled to test the electrochemical performance, with activated materials acting as the positive, activated carbon (AC) as the negative electrode. All the electrochemical measurements were recorded on using 3 M KOH aqueous electrolyte. EIS measurements were collected in the frequency range from 0.01 to 10^5 Hz at open circuit potential with a sinus amplitude of 5 mV.

3. Calculation Section

The specific capacitance of electrode materials was calculated by the following equation (1) and equation (2):[1]

$$E_{\mathrm{int}/D} = I \int_{t(U_{\max})}^{t(U_{\min})} U(t)dt \tag{1}$$

$$C_{\mathrm{int}/D} = \frac{2E_{\mathrm{int}/D}}{U_{\max}^2} \tag{2}$$

Where $E_{int/D}$ is the energy density (Wh kg^{-1}), I is the discharge current, U is the potential range (V), t is the discharge time (s), $C_{int/D}$ is the specific capacitance (F g^{-1}). Energy density and power density of the **PG-BBT** are evaluated according to equation (3) and equation (4), respectively:

$$E = \frac{1}{2} C_{sp} V^2 \tag{3}$$

$$P = \frac{E}{\Delta t} \tag{4}$$

where E stands for the energy density (Wh kg^{-1}), C_{sp} represents the specific capacitance (F g^{-1}), V refers to the potential window (V), P is the power density (W kg^{-1}) and Δt is the discharge time (S).

4. Experimental section

Synthesis of Ni-COF

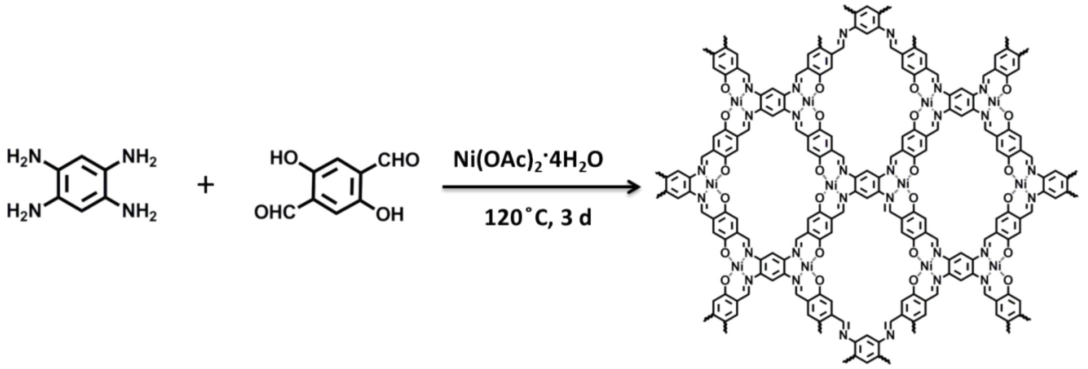

A glass bottle (volume of ca. 10 mL) was charged with 1,2,4,5-benzenetetraamine tetrahydrochloride (BTA) (20 mg, 0.07 mmol), 2,5-dihydroxy-1,4-benzenedicarboxaldehyde (HBC) (27.4 mg, 0.14 mmol), excess $Ni(OAc)_2 \cdot 4H_2O$, 0.5 mL of mesitylene and 1.5 mL of 1,4-dioxane. The resulting solution was sonicated for 10 minutes to obtain a homogenous dispersion. The glass bottle was transferred into a 25 mL Teflon-lined stainless steel autoclave. The autoclave was sealed and heated at 120 °C for 3 days and cooled to room temperature. The formed black precipitate was collected by filtration and washed with THF (3 × 20 mL), DMF (3 × 20 mL) and MeOH (3 × 20 mL), Soxhlet extracted by THF 24 h, then dried at 80 °C under vacuum for 24 h to give a black powder with 86% yield. FT-IR (powder): $v_{\max}$ 3281, 2566, 1621, 1563, 1508, 1435, 1372, 1295, 1227, 1127, 1056, 1001, 866, 801, 676, 612 and 558 cm^{-1}.

Synthesis of Ni_0-COF

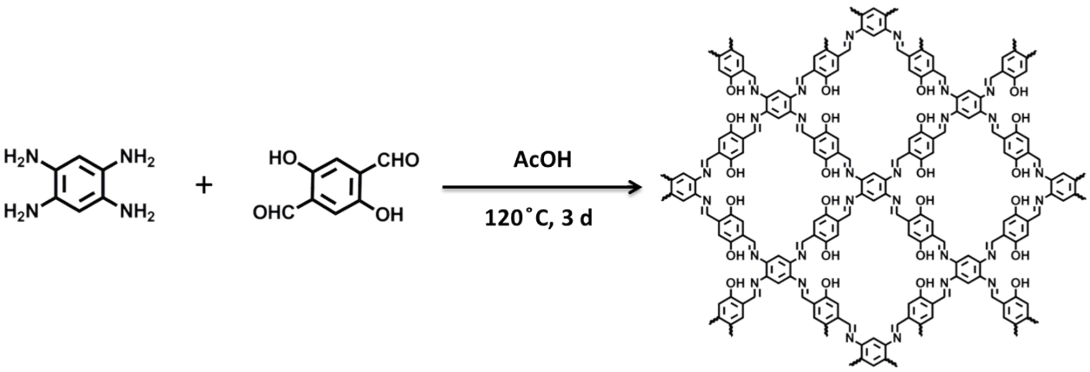

A glass bottle (volume of ca. 10 mL) was charged with 1,2,4,5-benzenetetraamine tetrahydrochloride (BTA) (20 mg, 0.07 mmol), 2,5-dihydroxy-1,4-benzenedicarboxaldehyde (HBC) (27.4 mg, 0.14 mmol), 0.5 mL of mesitylene and 1.5 mL of 1,4-dioxane. The resulting solution was sonicated for 10 minutes to obtain a homogenous dispersion, and then added 0.2 mL of 3 M aqueous acetic acid (AcOH). The glass bottle was transferred into a 25 mL Teflon-lined stainless steel autoclave. The autoclave was sealed and heated at 120 °C for 3 days and cooled to room temperature. The formed brown precipitate was collected by filtration and washed with THF (3 × 20 mL), DMF (3 × 20 mL) and MeOH (3 × 20 mL), Soxhlet extracted by THF 24 h, then dried at 80 °C under vacuum for 24 h to give a black powder with 81% yield. FT-IR (powder): ν_{max} 3072, 1621, 1576, 1492, 1431, 1358, 1281, 1258, 1202, 1157, 968, 857, 797, 743, 670 and 617 cm^{-1}.

5. Characterization

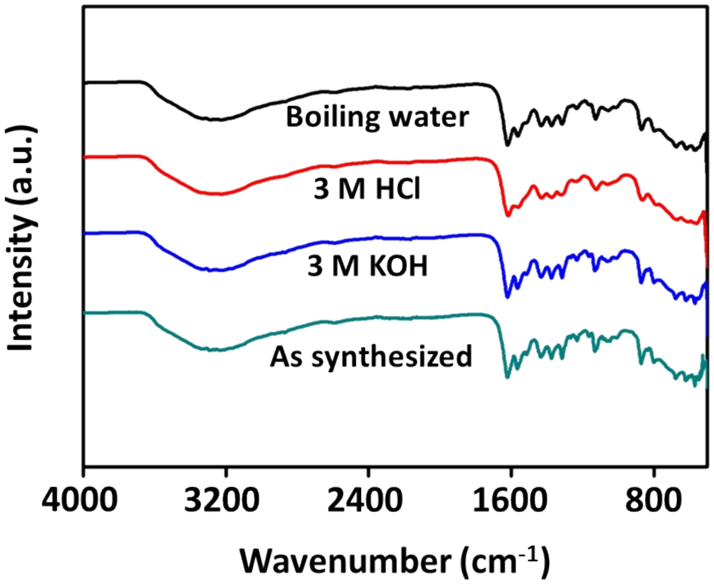

Fig. S1 Chemical stability tests of **Ni-COF**. The FT-IR patterns of **Ni-COF** treated for 5 days in different solvents.

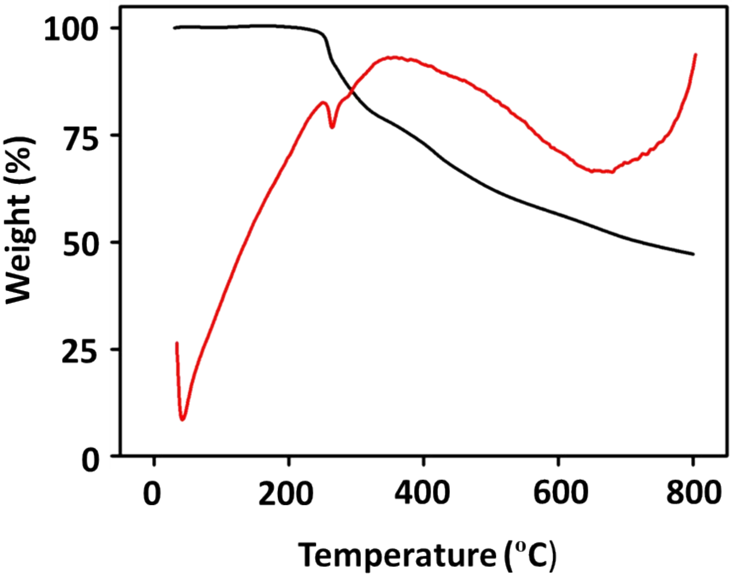

Fig. S2 Thermogravimetric analysis (TGA) curve of **Ni-COF**.

Ni-COF exhibited no discernible weight loss from 0 to 253 °C, and then **Ni-COF** started to decompose. At 800 °C, there was still 53% of weight residual for **Ni-COF**, indicating its excellent thermal stability.

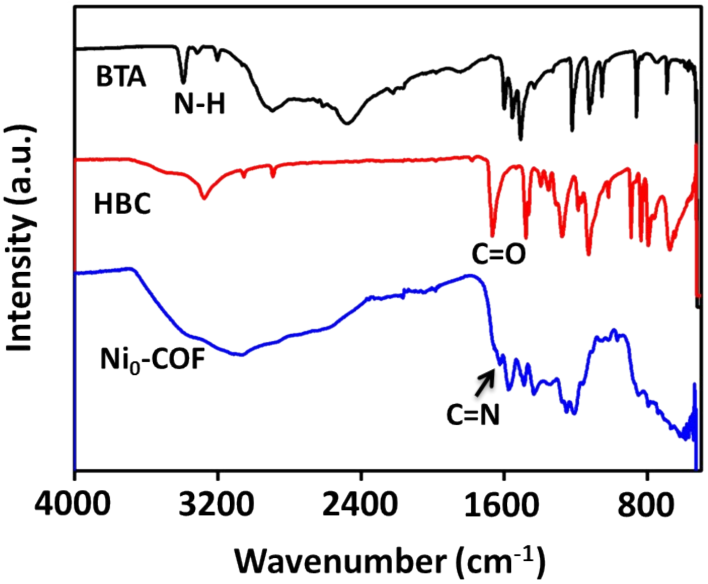

Fig. S3 FT-IR spectra of BTA, HBC and **Ni_0-COF**.

The disappearance of the characteristic C=O vibration band (1654 cm^{-1}), N-H vibration band (3389-3197cm^{-1}), and the appearance of C=N bonding (1621 cm^{-1}), indicates the formation of **Ni_0-COF**.

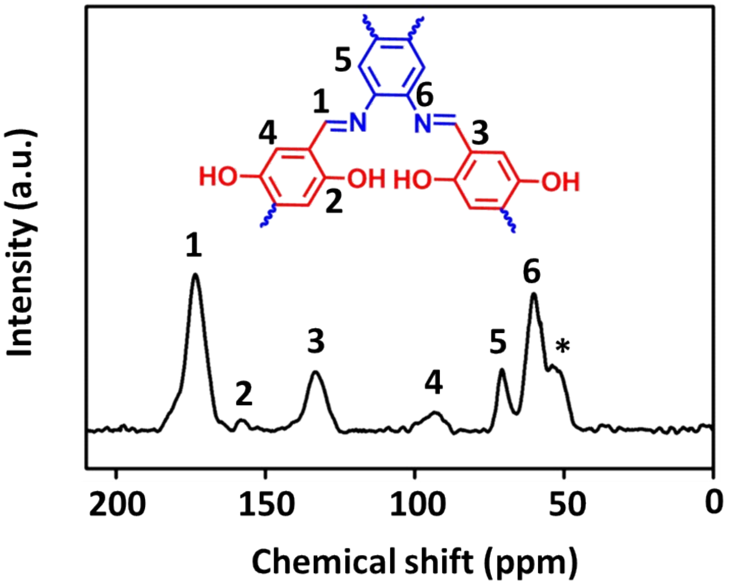

Fig. S4 Solid-state ^{13}C NMR spectrum of **Ni_0-COF**.

The characteristic resonance signal at 173 and 156 ppm is assigned to the C=N and C-O groups, respectively, which clearly reveals the formation of **Ni_0-COF**.

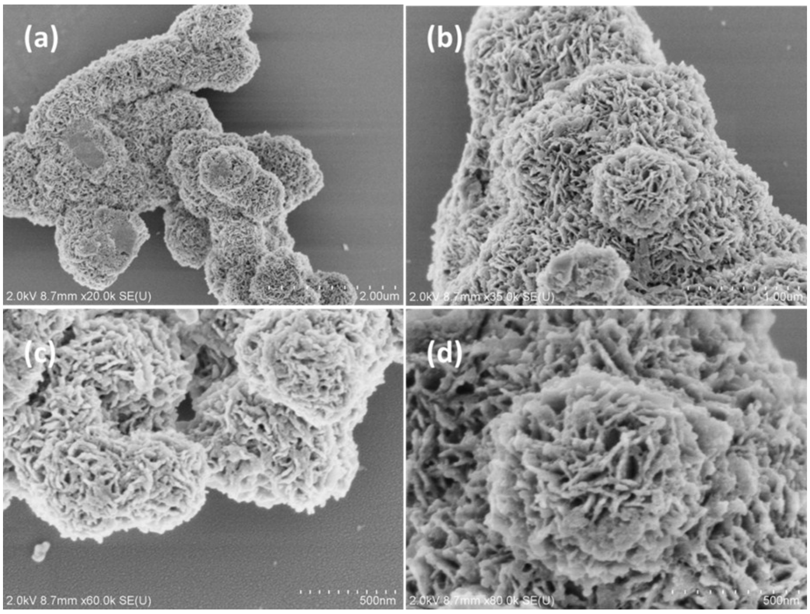

Fig. S5 SEM of **Ni-COF**.

The SEM images of **Ni-COF** show a spherical flower-like morphology, which is composed of numerous sheets.

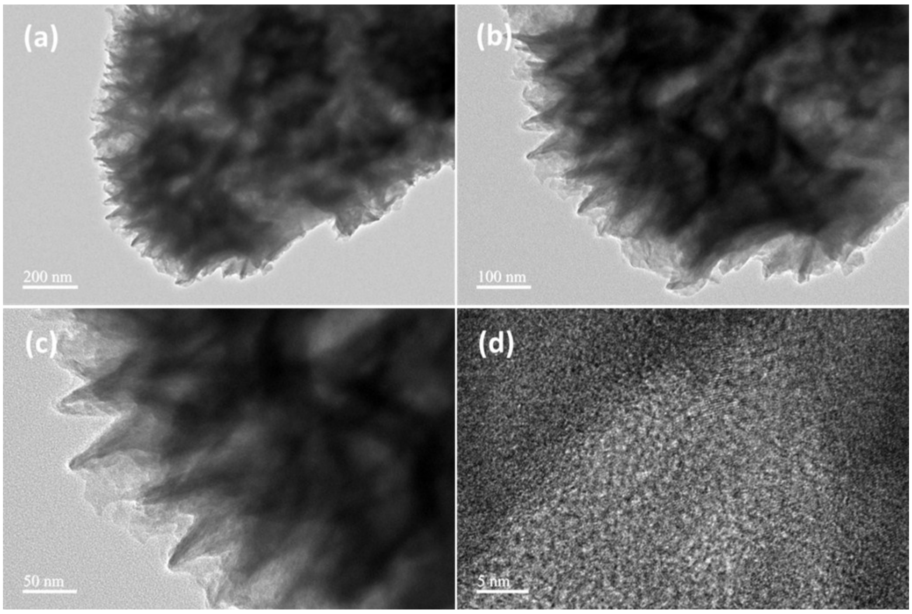

Fig. S6 TEM of **Ni-COF**.

TEM images clearly clarify that **Ni-COF** shows optically translucent feature owing to thick layer structure.

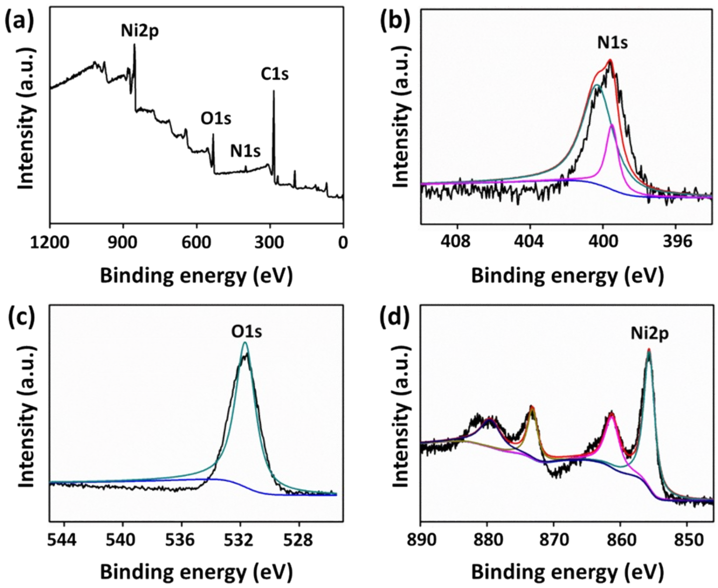

Fig. S7 XPS measurements of **Ni-COF**: (a) survey, (b) N 1s, (c) O 1s and (d) Ni 2p spectrum.

The XPS survey of Ni-COF confirms the presence of C, N, O and Ni. The signals at 399 and 532 eV correspond to N 1s and O 1s, respectively. The Ni 2p spectrum exhibits two main peaks around 856.1 and 873.6 eV that are assigned to Ni $2p_{3/2}$ and Ni $2p_{1/2}$, respectively, together with their corresponding satellite peaks around 861.3 and 880.1 eV.

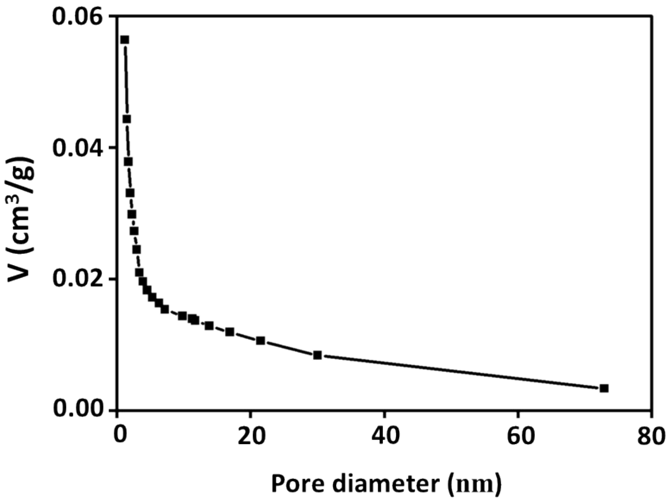

Fig. S8 Pore volume plot of **Ni-COF**.

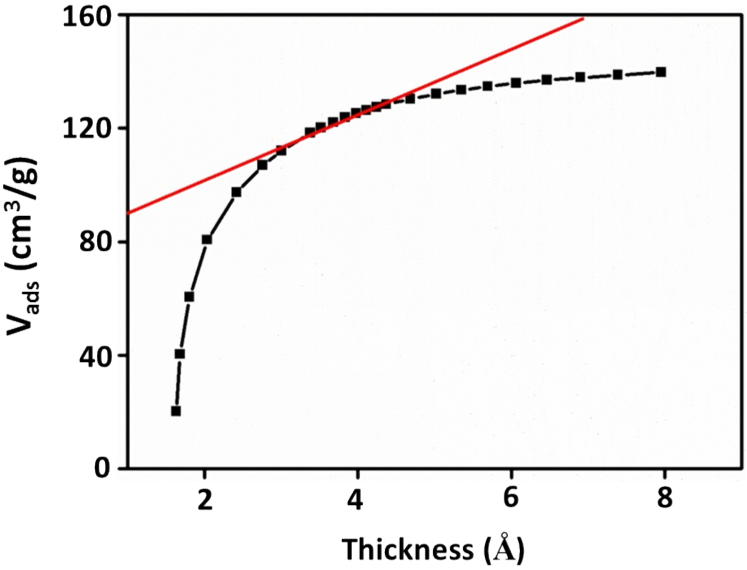

Fig. S9 t-Plots of **Ni-COF** using the Harkins and Jura reference isotherm. The lines represent the fit to the linear region, which is marked by the red symbols.

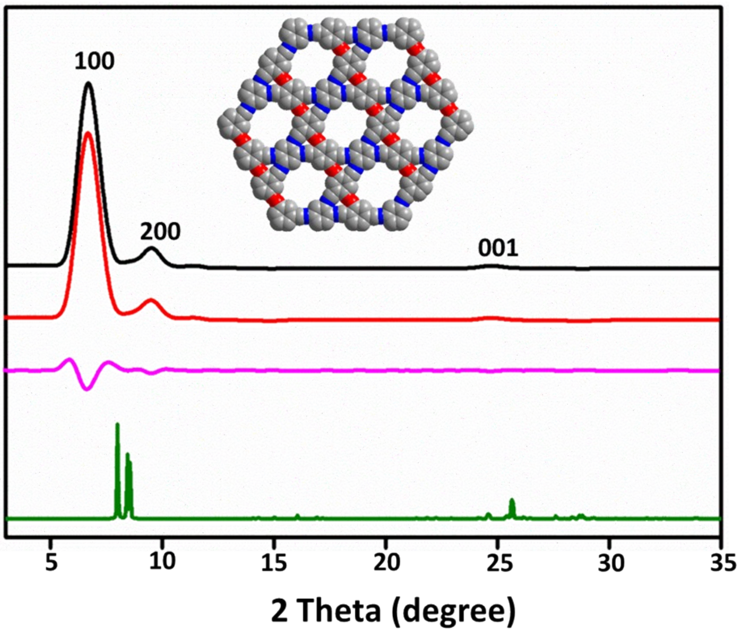

Fig. S10 PXRD patterns of **Ni$_0$-COF** with the experimental PXRD profiles in black, Pawley-refined profiles in red, calculated profiles in green, and the differences between the experimental and refined PXRD patterns in pink.

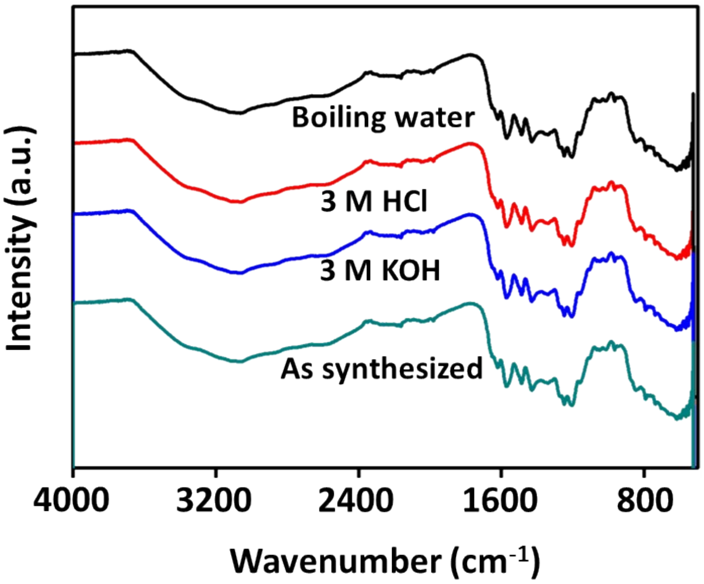

Fig. S11 Chemical stability tests of **Ni_0-COF**. The FT-IR patterns of **Ni_0-COF** treated for 5 days in different solvents.

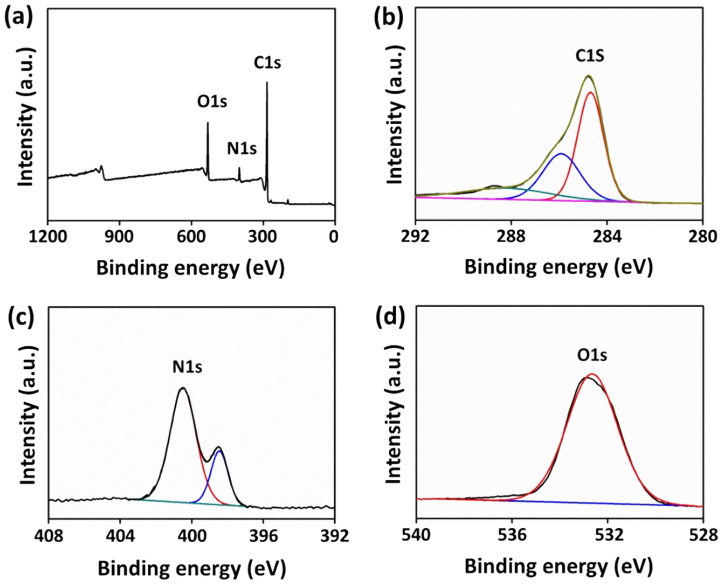

Fig. S12 XPS measurements of **Ni_0-COF**: (a) survey, (b) C1s, (c) N 1s and (d) O 1s spectra.

The XPS survey of **Ni_0-COF** confirms the presence of C, N and O. The signals at 284.8, 400.4 and 532.9 eV correspond to C1s, N 1s and O 1s, respectively.

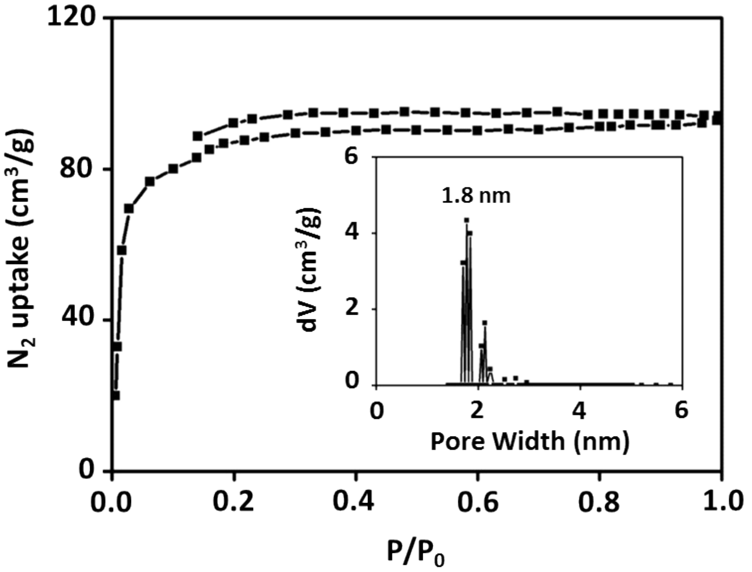

Fig. S13 Nitrogen adsorption-desorption isotherm of Ni_0-COF, and the insert exhibits the pore size distribution.

The curve displays a typical type-I shape with a sharp uptake under low relative pressure ($P/P_0 < 0.01$), indicating its microporous nature. The BET surface area of **Ni_0-COF** is estimated to be 258 m^2 g^{-1}. The average pore size of **Ni_0-COF** is 1.8 nm.

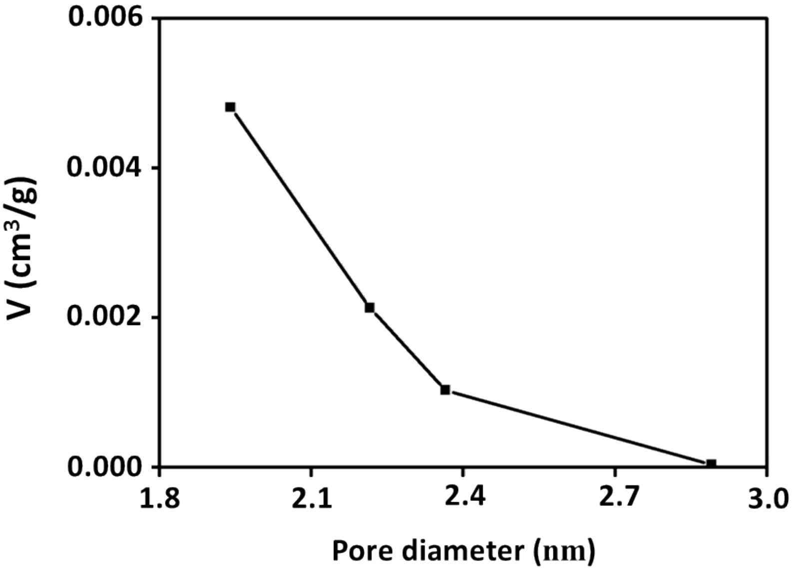

Fig. S14 Pore volume plot of **Ni_0-COF**.

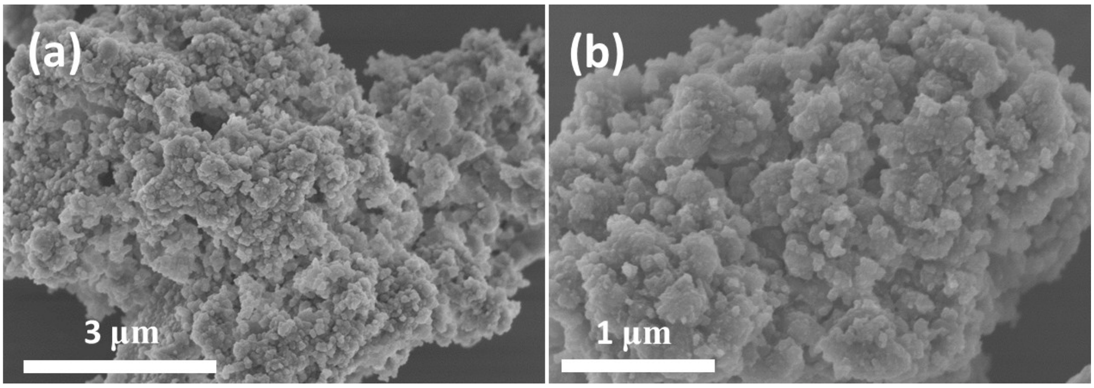

Fig. S15 SEM of **Ni_0-COF**.

The SEM images show a homogeneous morphology, which was consisted of a large number of grains.

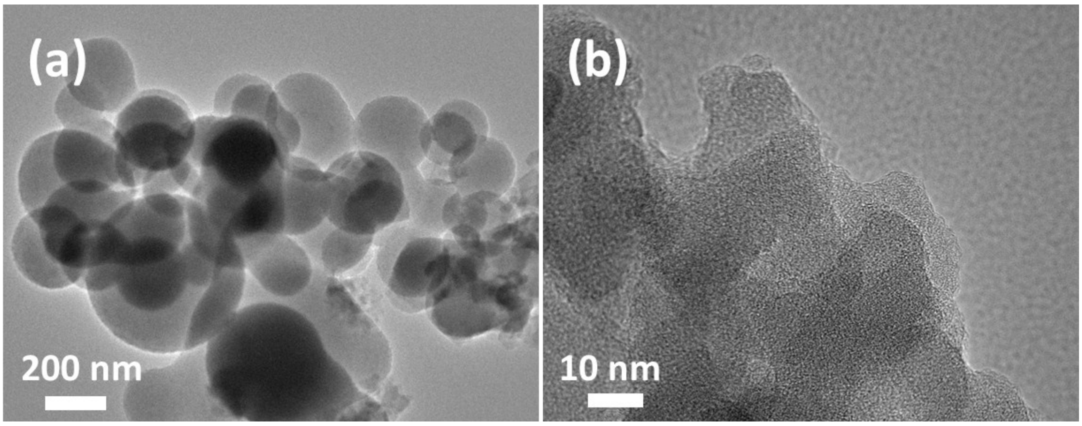

Fig. S16 TEM of **Ni_0-COF**.

The TEM images clearly observe that **Ni_0-COF** exhibits spherical grains and layer-by-layer structure.

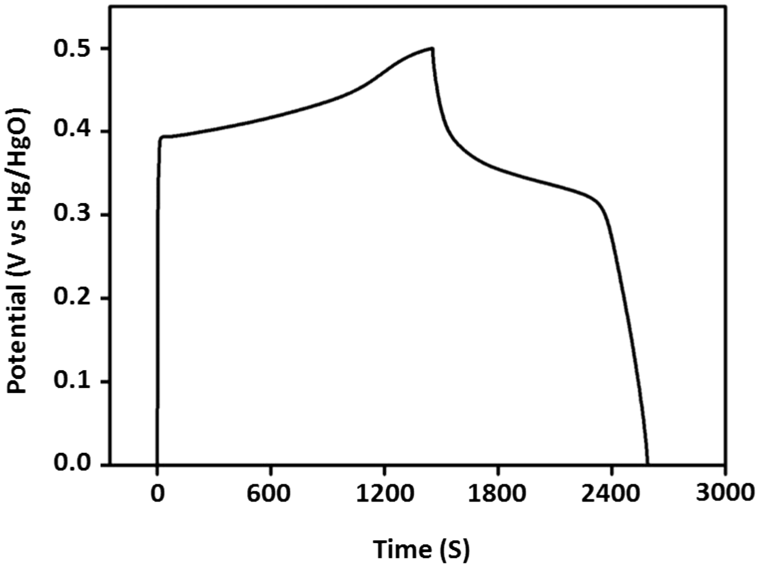

Fig. S17 GCD curve of **Ni-COF** at 0.5 A g^{-1}.

The specific capacitance of **Ni-COF** is calculated to be 1478 F g^{-1} at 0.5 A g^{-1}.

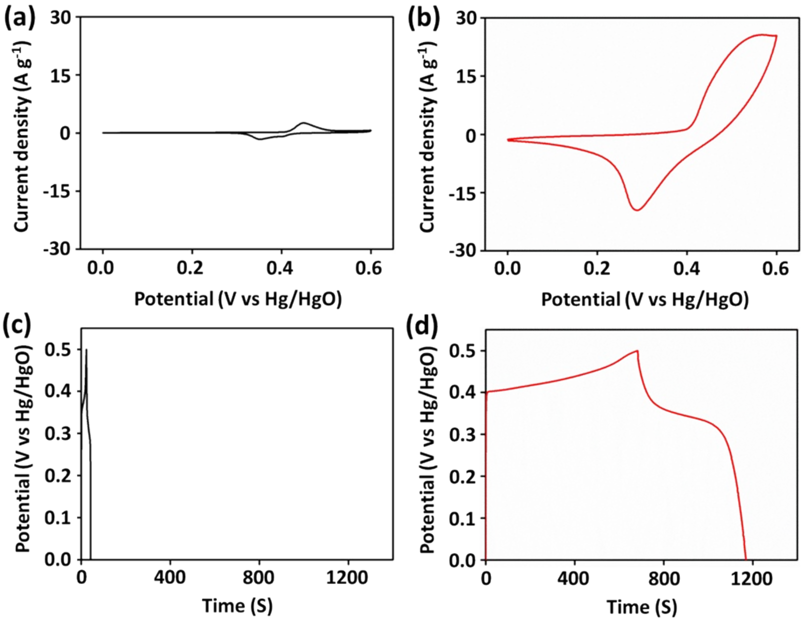

Fig. S18 CV curves of (a) Ni foam and (b) **Ni-COF** at 5 mV s^{-1}. GCD curves of (c) Ni foam and (d) **Ni-COF** at 1 A g^{-1}.

To preclude the impact of Ni foam substrate on the performance, electrochemical experiment on it was conducted (48 F g^{-1} at 1A g^{-1}). Compared with **Ni-COF** (1257 F g^{-1} at 1 A g^{-1}), the contribution from the Ni foam substrate to the total capacity is negligible.

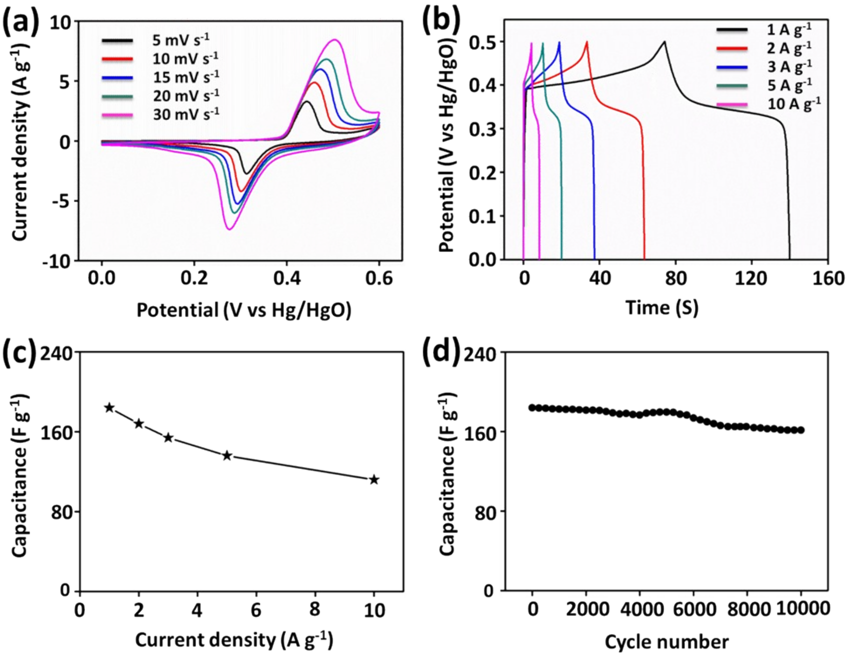

Fig. S19 Electrochemical properties of **Ni_0-COF** in a three-electrode system. (a) CV curves at scan rates from 5 to 30 mV s^{-1}. (b) GCD curves at different current densities (1-10 A g^{-1}). (c) Capacitance vs current density. (d) Cyclic stability measurement at a current density of 1 A g^{-1}.

The CV curves exhibit different scan rates from 5 to 30 mV s^{-1} and display a pair of redox peaks, indicating the pseudocapacitive behaviour. The GCD profiles show different current densities from 1 to 10 A g^{-1}. The GCD curves show a severely distorted triangular shape, which is resulted from the typical pseudocapacitive behaviour, in agreement with the CV analyses. The discharging capacitances of **Ni_0-COF** are calculated to be 184, 168, 154, 136 and 112 F g^{-1} at 1, 2, 3, 5 and 10 A g^{-1}, respectively. The specific capacitance at 10 A g^{-1} retains 61% of that at 1 A g^{-1}, indicating its good rate capability. The stability test of the **Ni_0-COF** electrode was evaluated at 1 A g^{-1}. It demonstrates high stability with high capacitance retention of 87.5 % after 10000 cycles.

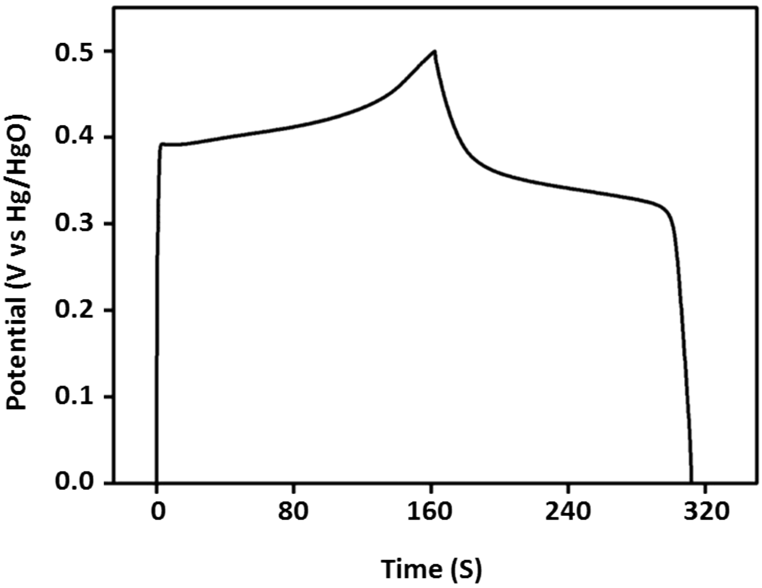

Fig. S20 GCD curve of **Ni_0-COF** at 0.5 A g^{-1}.

The specific capacitance of **Ni_0-COF** is calculated to be 204 F g^{-1} at 0.5 A g^{-1}.

Table S1. Fractional atomic coordinates for the triclinic *P*1/(1) unit cell of **Ni-COF** calculated using the Materials Studio 7.0.

Ni-COF			
Triclinic *P*1/(1) a = 12.8777 Å, b = 12.1493 Å, c = 14.8164 Å			
C1	1.12607	1.09325	-0.34932
C2	0.19516	1.04500	-0.28450
C3	0.08888	0.01325	0.89411
C4	-0.08759	0.01475	0.01845
C5	0.83769	0.05471	-0.03641
C6	0.95110	1.09874	-0.22850
N7	-0.19843	-0.05550	0.23180
C8	-0.30027	0.05432	1.25405
C9	-0.14787	0.28604	1.06463
C10	0.06568	0.38215	-0.10817
C11	0.19392	0.60524	0.71894
C12	0.11821	0.73890	0.70731
C13	-0.09166	0.64556	0.87511
C14	-0.22250	0.41979	1.05298
C15	0.20979	0.90225	0.61688
N16	0.18645	1.08387	0.52606
O17	0.15807	0.26699	-0.11881
O18	-0.18603	0.75377	0.89622
N19	0.18645	0.11717	-0.27905
C20	0.67973	0.05196	0.89536
C21	0.59246	0.03926	0.87628
C22	0.34446	-0.09644	0.13816

C23	0.24332	-0.12747	1.14688
C24	0.39008	-0.03002	0.89774
C25	0.64095	0.11375	0.62821
C26	0.74477	0.15176	0.61286
C27	0.26786	-0.12468	0.95940
N28	0.13234	-0.04848	0.99266
Ni29	1.08812	0.19514	0.43073
O30	-0.01515	-0.29032	0.43887
O31	1.00377	0.31728	0.31835
Ni32	1.89884	1.83119	1.32795

Table S2. Fractional atomic coordinates for the triclinic P1/(1) unit cell of **Ni$_0$-COF** calculated using the Materials Studio 7.0.

Ni$_0$-COF			
Triclinic P1/(1) *a* = 12.9144 Å, *b* = 12.4401 Å, *c* = 22.1318 Å			
C1	1.02688	0.82450	-0.08070
C2	0.09651	0.81008	-0.05189
C3	0.07812	-0.08066	0.95399
C4	-0.01143	0.06066	-0.07444
C5	0.90331	0.07226	-0.09593
C6	0.91337	0.94356	-0.09096
N7	-0.00042	0.18851	-0.09024
C8	-0.05438	0.35796	0.86442
C9	-0.02392	0.47331	0.85173
C10	0.07117	0.42719	-0.12226
C11	0.12044	0.57646	0.84158
C12	0.01958	0.71919	0.82860
C13	-0.06181	0.77289	0.79567
C14	0.08956	0.66065	0.79993
C15	0.10287	0.66450	0.86234
N16	-0.01906	0.77279	0.90680
O17	0.14064	0.27534	-0.08742
O18	-0.11796	0.92781	0.76363
N19	-0.18548	-0.06899	-0.09161
C20	0.71214	0.04998	0.88960
C21	0.58584	0.02849	0.90778
C22	0.33677	0.15746	0.91906

C23	0.28979	-0.00167	0.96692
C24	0.27058	-0.27046	1.11021
C25	0.52734	-0.12813	0.95580
C26	0.19029	-0.09786	1.00840
N27	0.15148	-0.02085	0.94453
O28	0.25771	0.26200	-0.11447
O29	0.64421	-0.20875	0.91613
C30	1.47478	1.16777	0.90158

6. Reference

[1] A. Laheäär, P. Przygocki, Q. Abbas, F. Béguin, *Electrochem. Commun.*, 2015, **60**, 21-25.